AIAA JOURNAL
Vol. 37, No. 4, April 1999

Unsteady Drag Consideration in Stochastic Eulerian–Lagrangian Formulation of Two-Phase Flow

Keh-Chin Chang* and Jinn-Cherng Yang†
National Cheng-Kung University, Tainan 70101, Taiwan, Republic of China

The unsteady effect of drag coefficient in the stochastic Eulerian–Lagrangian computation of a two-phase, turbulent, planar mixing layer flow of droplets-in-gas type is examined. It is found that the use of an unsteady drag coefficient in modeling two-phase turbulent flows with the stochastic Eulerian–Lagrangian formulation is necessary to obtain complete information of the dispersed-phase turbulence characteristics. It is shown that the use of the quasisteady drag coefficient, which is mostly adopted in two-phase turbulent flow computations, does not cause too much deviation in the determination of mean quantities of the droplet velocity through use of the ensemble-averaging method weighting with the probability density function of the carrier phase.

Nomenclature

C_D = drag coefficient
D = drag force
D/Dt = substantial derivative
d_p = droplet diameter, μm
F = force
g = gravity
K = history-force kernel
n = number density, number of droplets per cubic meter
P = value of probability density function
Re = droplet Reynolds number, $(\rho|\Delta \boldsymbol{U}|d_p)/\mu$
t = time, s
t_M = dimensionless time defined by Mei[13]
U, u = instantaneous and mean velocities, respectively, m/s
V = freestream velocity with respect to stationary droplet
α_{12} = velocity ratio of two neighboring grid cells
Δt = time increment
ΔU = velocity slip, $|U - U_p|$
$\delta(t)$ = Dirac delta function, 0 for $t \neq 0$ and

$$\int_{0^-}^{0^+} \delta(\tau)\, \mathrm{d}\tau = 1$$

ρ = density, kg/m^3
τ_p, τ_r = dynamic relaxation time and residence time of droplet, respectively
ϕ = factor accounting for deviation from the Stokesian drag

Subscripts

i = ith direction
in = inlet
p = dispersed phase
s = Stokesian drag
1, 2 = upstream and downstream, respectively

Superscripts

$'$ = fluctuation
$\bar{}$ = ensemble-averaging value

I. Introduction

THE Eulerian–Lagrangian method is commonly used in the simulation of two-phase turbulent flows in engineering applications. This hybrid method consists of the Eulerian formulation for the carrier phase coupled with the Lagrangian formulation for the dispersed phase. Recent comprehensive reviews on two-phase flow models can be found in Refs. 1–3. Currently, the most popular numerical method to simulate droplet dispersion in turbulence is the stochastic (Monte Carlo) approach, which was originally developed by Gosman and Ioannides.[4] In the conventional stochastic Eulerian–Lagrangian method, the dispersed-phase properties at a grid node are determined using ensemble averaging of the properties of many individual droplets (or particles, per se) in which their trajectories fall within the grid cell. Therefore, it is required to track a great number of trajectories to attain a statistically stationary solution.[5] Recently, Dutta et al.[6] proposed a discrete probability function (DPF) method for droplet dispersion computation that is capable of providing accurate simulations with low statistical noise. The DPF and conventional stochastic approaches differ in the way that the information concerning probability is stored in the DPF method. However, the need for a larger number of computational droplets makes the DPF method more expensive than the conventional stochastic method. Chen and Pereira[7,8] developed a stochastic-probabilistic dispersion model for the prediction of two-phase turbulent flow that can significantly improve the computational efficiency of the stochastic Lagrangian computation by reducing the number of trajectories to be tracked. However, both the conventional stochastic method and the stochastic-probabilistic method developed by Chen and Pereira[7] involve the solution of the Lagrangian equation of instantaneous motion. Usually, the quasisteady formula of the drag coefficient is employed in the formulation of the Lagrangian equation of instantaneous motion associated with the stochastic approach for two-phase turbulent flows.[5,7] In the analysis of Chang et al.[9] based on the conventional stochastic method, it was found that the use of the quasisteady formula of the drag coefficient in the Lagrangian equation of instantaneous motion could cause significant errors in the predictions of the probability density functions (PDFs) of dispersed-phase velocity fluctuations, particularly for large droplets. A similar observation was reported in the recent study of Chen and Pereira.[8] The reason is as follows: The Lagrangian equation of instantaneous motion in the ith direction is conventionally simplified as

$$\frac{\mathrm{d}U_{pi}}{\mathrm{d}t} = \frac{U_i - U_{pi}}{\tau_p} + g_i \tag{1}$$

where the droplet dynamic relaxation time, which denotes a characteristic time of the droplet reaching its dynamic equilibrium with the carrier phase, is defined by

$$\tau_p = \frac{4 d_p \rho_p}{3 C_D \rho |\Delta \boldsymbol{U}|} \tag{2}$$

and the instantaneous velocity of the carrier phase is given by

$$U_i = u_i + u_i' \tag{3}$$

Received Sept. 9, 1998; revision received Dec. 7, 1998; accepted for publication Dec. 7, 1998.

*Professor, Institute of Aeronautics and Astronautics. E-mail: kcc@mail.iaa.ncku.edu.tw. Senior Member AIAA.
†Graduate Student, Institute of Aeronautics and Astronautics.

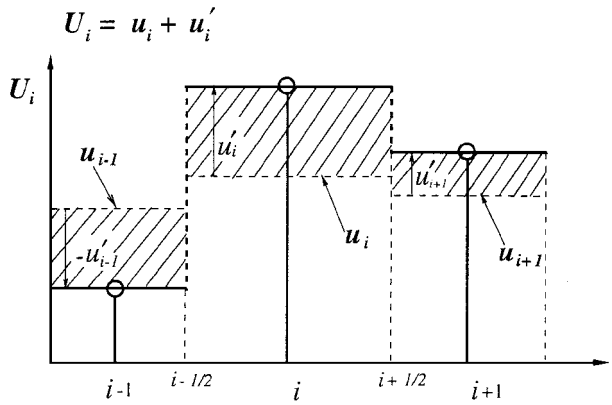

Fig. 1 Discretization of the instantaneous carrier-phase velocity in the stochastic calculation procedure.

Here C_D is the quasisteady drag coefficient usually expressed in the form

$$C_D = (C_D)_s \, \phi(Re) \tag{4}$$

where $(C_D)_s$ denotes the Stokesian drag coefficient defined by

$$(C_D)_s = 24/Re \tag{5}$$

The factor $\phi(Re)$ of Eq. (4) accounts for deviation from the Stokesian drag coefficient when the condition of $Re \ll 1$ is not met. Many forms of $\phi(Re)$ at different ranges of Reynolds number can be found in Ref. 10.

In contrast, the Eulerian framework is used to formulate the carrier-phase transport equations. To obtain the solutions of the Eulerian transport equations, the finite volume method, which adopts the control-volume formulation and lends itself to conservation laws, is widely used in numerical analysis. The basic idea of the discretization process is that the calculation domain is divided into a number of nonoverlapping control volumes (cells), each surrounding a grid node. Uniformly distributed flow properties are usually assumed inside the cell of a grid node. The mean carrier-phase velocity u_i shown in Eq. (3) is obtained from the solution of its corresponding Reynolds-averaged, Eulerian transport equation for a given grid cell in the stochastic calculation procedure. Thus, as a droplet (dispersed-phase element) passes through a grid cell to its neighboring grid cell, it encounters a remarkable step change of the instantaneous carrier-phase velocity at the interface of these two grid cells, which is caused by the discretization process and, mostly, from the different fluctuating carrier-phase velocities determined in the stochastic calculation procedure for each grid cell (schematically shown in Fig. 1). As a result, the unsteady effect of drag coefficient has to be considered in Eq. (1) except under a special condition in which the residence time of the droplet passing through a grid cell is long enough, as compared to its dynamic relaxation time, so that the droplet can closely approach its steady-state condition in the grid cell. According to the analysis given by Chang et al.,[9] this special condition is not usually met, particularly for large droplets, in their tested spray problems.

The objective of this work is to reevaluate the Eulerian–Lagrangian formulation associated with the conventional stochastic calculation procedure, by using an unsteady expression of the drag coefficient, against measurements in a well-defined, two-phase flow problem: that of a turbulent mixing layer flow loaded with polydispersed droplets.

II. Unsteady Drag

Michaelides[11] reviewed progress of the analytical studies of the transient equation of motion of a droplet for finite droplet Reynolds numbers. Michaelides[11] summarized that very few theoretical expressions of drag are available at Reynolds number values higher than that of creeping flow. Further, if effects such as freestream turbulence and unsteadiness are added to the problem, our understanding of drag response is still fragmentary, especially at high droplet Reynolds numbers.

Sano[12] was the first to succeed in deriving an expression for the unsteady drag on a sphere in which the asymptotic expansion type of solution was presented for an impulsively started motion (from rest) at small Reynolds number correct to $\mathcal{O}(Re^2)$. The unsteady drag coefficient of a sphere for $t > 0$ is given by

$$\frac{C_D}{(C_D)_s} = 1 + \frac{1}{3}\delta(t_M) + \frac{3}{16}Re\left[\left(1 + \frac{16}{Re^2 t_M^2}\right)\mathrm{erf}\left(\frac{1}{2}\sqrt{\frac{Ret_M}{2}}\right) + 2\sqrt{\frac{2}{\pi Ret_M}}\left(1 - \frac{4}{Ret_M}\right)\exp\left(-\frac{Ret_M}{8}\right)\right] + \frac{9}{160}Re^2 \ell n\left(\frac{1}{2}Re\right) + \mathcal{O}(Re^2) \tag{6}$$

with dimensionless time

$$t_M = 2\Delta U(t/d_p) \tag{7}$$

The transient (time-dependent) part of Sano's solution decays more quickly, as the inverse square of time (known as intermediate-time behavior[13]), than the conventional $t^{-1/2}$ rate (known as short-time behavior), at long times. Nevertheless, according to the numerical and analytical studies of Mei,[13] as well as Lovalenti and Brady,[14,15] the existence of such an exponential decay of the drag at long times was revealed. Further, the condition of an impulsively started (from rest) motion imposed on Sano's solution is rarely met in practical two-phase flows.

Mei and Adrian[16] obtained another expression for the total unsteady drag (except the external force) in rectilinear motion at finite Reynolds numbers for a stationary sphere experiencing a small fluctuation in the freestream velocity V as follows:

$$\mathrm{D}(t) = F_{\mathrm{qs}}(t) + F_H(t) + F_{\mathrm{am}}(t) + F_{\mathrm{fs}}(t) \tag{8}$$

where F_{qs} is the quasisteady drag if the acceleration of the flow is vanishingly small, F_H is the history (or Basset) force due to the effects of the deviation of the flow from a steady flow pattern around the sphere, F_{am} is the added-mass (or virtual-mass) force related to the instantaneous acceleration, and F_{fs} is due to the unsteadiness and spatial nonuniformity of the freestream velocity. These forces are given, respectively, as

$$F_{\mathrm{qs}}(t) = 3\pi\mu d_p V(t)\phi(Re) \tag{9}$$

$$F_H(t) = 3\pi\mu d_p \int_{-\infty}^{t} K(t-\tau)\frac{\mathrm{d}V}{\mathrm{d}\tau}\,\mathrm{d}\tau \tag{10}$$

$$F_{\mathrm{am}}(t) = \frac{1}{12}\rho\pi d_p^3 \frac{\mathrm{d}V}{\mathrm{d}t} \tag{11}$$

$$F_{\mathrm{fs}}(t) = \frac{1}{6}\rho\pi d_p^3 \frac{\mathrm{D}V}{\mathrm{D}t} \tag{12}$$

where $K(t-\tau)$ is the history-force kernel, which is generally a function of droplet Reynolds number and Strouhal number. Consider an unsteady flow over a sphere due to a sudden change in the freestream velocity, from V_1 to V_2 (here $V = \Delta U$) as the sphere crosses the interface of two neighboring grid cells, at $t = 0$. Incorporated with the uniform distribution assumption of flow properties inside a grid cell, $\mathrm{D}V/\mathrm{D}t = \mathrm{d}V/\mathrm{d}t$, and the acceleration is $\mathrm{d}V/\mathrm{d}t = \Delta V\delta(t)$ with $\Delta V = V_2 - V_1$. The forces F_{am} and F_{fs} can be now rewritten as

$$F_{\mathrm{am}}(t) = \tfrac{1}{12}\rho\pi d_p^3 \Delta V\delta(t) \tag{11'}$$

$$F_{\mathrm{fs}}(t) = \tfrac{1}{6}\rho\pi d_p^3 \Delta V\delta(t) \tag{12'}$$

For $t > 0$, the preceding flow condition leads to the following expressions for F_{qs} and F_H:

$$F_{\mathrm{qs}}(t) = 3\pi\mu d_p V_2\phi(Re) = 3\pi\mu d_p \Delta U_2\phi(Re) \tag{9'}$$

$$F_H(t) = 3\pi\mu d_p \int_0^t K(t-\tau)\Delta V\delta(\tau)\,\mathrm{d}\tau = 3\pi\mu d_p(\Delta U_2 - \Delta U_1)K(t) \tag{10'}$$

The total drag on the sphere as defined in Eq. (8) for $t > 0$ is, thus,

$$\frac{\mathrm{D}(t)}{3\pi\mu d_p \Delta U_2} \equiv \frac{C_D(t)}{(C_D)_s} = (1-\alpha_{12})K(t) + \phi(Re) \tag{13}$$

where

$$\alpha_{12} = \Delta U_1 / \Delta U_2 \tag{14}$$

Therefore, the simplified form of the Lagrangian equation of instantaneous motion, i.e., Eq. (1), is still valid in the two-phase flow calculation with the stochastic approach provided that the effective drag coefficient accounting for the unsteady effects, as shown in Eq. (13), is used. Equation (13) takes the form identical to Eq. (4) for $t \gg 1$ because the history-force kernel asymptotically approaches zero value at an infinitely long time.

The evaluation of the history-force kernel is not trivial. Mei and Adrian[16] proposed the following curve-fit approximation for the history-force kernel based on the numerical results of the unsteady flows over a sphere with small fluctuations in the freestream velocity and an asymptotic analysis of the same flow at small Reynolds numbers:

$$K(t-\tau) = \left(\left[\frac{4\pi\mu}{\rho d_p^2}(t-\tau) \right]^{\frac{1}{4}} + \left\{ \frac{\pi\rho}{\mu d_p} \left[\frac{V(\tau)}{f_H(Re)} \right]^3 (t-\tau)^2 \right\}^{\frac{1}{2}} \right)^{-2} \tag{15}$$

with

$$f_H(Re) = 0.75 + 0.105Re \tag{16}$$

In the study by Mei and Adrian,[16] the factor $\phi(Re)$ shown in Eq. (9) was chosen as one of the best correlations for $\phi(Re)$ compiled by Clift et al.[10]:

$$\begin{aligned} \phi(Re) &= 1 + \tfrac{3}{16}Re, && 0 < Re \le 0.01 \\ &= 1 + 0.1315Re^{0.82 - 2.171 \times 10^{-2} \ln Re}, && 0.01 < Re \le 20 \\ &= 1 + 0.1935Re^{0.6305}, && 20 < Re \le 260 \end{aligned} \tag{17}$$

For the history-force kernel proposed by Mei and Adrian,[16] the $t^{-1/2}$ (short-time) behavior is asymptotically correct, but the t^{-2} decay (intermediate-time behavior) is an artifact of the curve-fit procedure. It is consistent with Sano's result[12] but not with the results of Lovalenti and Brady,[14,15] which indicate explicitly exponential decay of the history-force kernel at long times, for small Reynolds numbers. Nevertheless, recent numerical results by Lawrence and Mei[17] support the qualitative features of Eq. (15), in particular the t^{-2} decay of the history-force kernel at long times, although there was indeed a short period around $t_M \sim 100$ when $K(t_M)$ decreased exponentially for the case of small Reynolds numbers. As concluded by Lawrence and Mei,[17] the history-force kernel proposed by Mei and Adrian,[16] i.e., Eq. (15), performed satisfactorily in the cases of $V_1 \ge 0$ and $V_2 > 0$, with a substantial quantitative error only when $K(t)$ itself is quite small and is, thus, overshadowed by $\phi(Re)$ in Eq. (13). Furthermore, it was agreed[16,17] that Sano's solution[12] for startup from rest ($\alpha_{12} = 0$), i.e., Eq. (6), performed very well as compared to the numerical solution in the low-droplet-Reynolds-number range. Thus, Eq. (13), combined with Eqs. (15) and (17), is used to determine the unsteady drag coefficient in the work except for the condition of $\alpha_{12} = 0$ and $Re \le 1$, in which Sano's solution [Eq. (6)] takes over the expression of unsteady C_D.

III. Problem Description and Model Analysis

Test Problem

The well-defined experiment of a droplet-loading, planar, mixing-layer flow in a vertical tunnel,[18,19] which is schematically shown in Fig. 2, is selected as the test problem. More details of the test problem and experimental methods can be found in Ref. 19. Thus, only a brief description of the test problem is given here. The tunnel was divided into two separate flow paths by an upstream central splitting plate. The mean velocities of the high- and low-speed streams were equal to 10.2 and 2.36 m/s, respectively. A Sono-Tek ultrasonic nozzle, located 950 mm upstream of the test section in the high-speed stream, generated polydispersed water droplets. The trailing edge of the splitting plate was extended 150 mm into the test section. A rectangular coordinate was selected such that the streamwise x coordinate is downward with the origin at the central separation point of the splitting plate, and the transverse y coordinate is positive toward the high-speed-stream side.

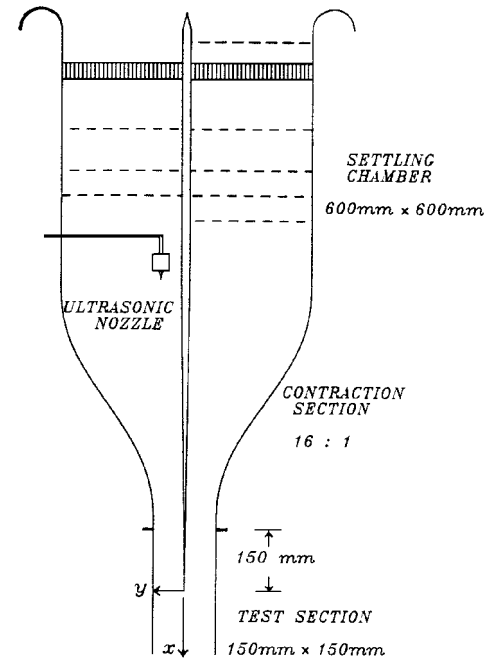

Fig. 2 Schematic of the test problem.

Measurements of the mean and fluctuating flow properties of the streamwise and transverse components for both phases were made using a two-component-phase Doppler particle analyzer. Eight sets of data labeled with the mean droplet sizes of 10, 20, 30, 40, 50, 60, 70, and 80 μm were recorded. A complete measurement at the streamwise station of $x = 5$ mm was made for the inlet condition required for the computations.

Physical Modeling

The boundary-layer approximation, which neglects the diffusion terms along the streamwise direction, is made for the carrier-phase (gas) flow in this investigated mixing-layer problem. The flowfield of the test problem is determined through use of the k–ε model. The applicability of the k–ε model in the simulation of this test problem has been demonstrated by Chang et al.[19] Because the volumetric fractions occupied by the droplets (dispersed phase) are less than 10^{-5} (in the interest of the computational domain), the present two-phase flow is rather dilute and the interactions among droplets are assumed to be negligible.

The dispersed phase is treated by tracking individual droplets as they move through the turbulence field of the carrier phase. To account for the effect of the size spectrum, the dispersed phase is represented by eight discrete droplets with the sizes of 10, 20, 30, 40, 50, 60, 70, and 80 μm, each characterizing a group of physical droplets that possess the same properties, such as size and velocity. For details of the problem modeling, see Ref. 19.

Numerical Solution Procedure

Computation of the carrier-phase flowfield is performed with the finite volume method using the SIMPLER algorithm and the power-law scheme.[20] The equation of motion of a droplet [Eq. (1)], which is a nonlinear first-order, ordinary differential equation, is solved using the Runge–Kutta method modified by Fehlberg.[21] Once a droplet reaches the dynamic equilibrium state with the carrier gas along its trajectory through a specified grid cell, the droplet velocity is set to be equal to the carrier-phase velocity until it leaves the grid cell.

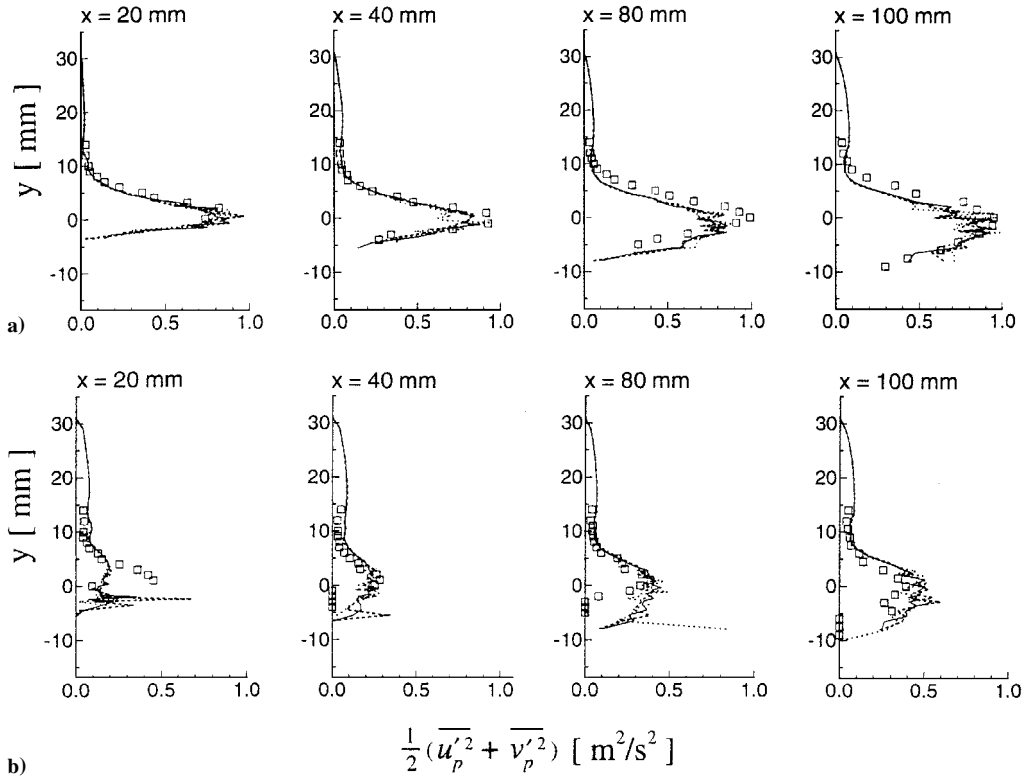

Fig. 3 Evolution of measured and three predicted $(\overline{u_p'^2} + \overline{v_p'^2})/2$ of the droplets, in conjunction with different numbers of computational droplets and by using the unsteady drag coefficient, for droplets with sizes of a) 10 and b) 80 μm: □, measurements[18]; ——, 10,000 drops/size; - - -, 8000 drops/size; and · · · ·, 3000 drops/size.

To obtain statistically significant properties of the dispersed phase for a given representative group of droplets, an adequate number of computational droplets of the same size, each corresponding to an instantaneous carrier-phase velocity as expressed in Eq. (3), has to be tracked in the stochastic Lagrangian computation. For a given fluctuating velocity u_i', which is randomly sampled in the solution procedure, at each integrating time step there exists a corresponding value of PDF, i.e., P. Because the measured U_i histograms exhibited Gaussian distribution form,[9] these PDFs are represented using Gaussian functions in the computations. It is evident that the use of a wider interval of the PDF domain in computation leads to a better simulation of droplet turbulent dispersion in the flowfield.[5] The present work uses the PDF interval bounded within $\pm 2(\overline{u_i^2})^{1/2}$, which is equivalent to 95.5% probability, in the simulation of the test problem. The mean value of the droplet velocity at a specified grid node is determined by using the ensemble-averaging concept:

$$u_{pi} = \frac{\sum_{m=1}^{M} n_m P_m (U_{pi})_m}{\sum_{m=1}^{M} n_m P_m} \tag{18}$$

where the index m is the mth computational droplet entering the control volume of the grid node. More information on and discussion of the numerical analysis employed in the work can be found in the papers of Chang and Wu[5] and of Chang et al.[19]

IV. Results and Discussion

Computation using the quasisteady drag coefficient based on the correlation shown in Eq. (17) is also performed to provide a baseline with which to compare the predictions using the unsteady drag coefficient already described. The previous study of Chang and Wu[5] revealed that the use of no fewer than 1000 computational droplets for each representative size in association with the conventional stochastic calculation procedure was able to yield a statistically stationary, mean quantity of the dispersed-phase velocity by means of the ensemble-averaging formulation of Eq. (18). However, remarkably more computational droplets are required in this study to obtain a statistically significant solution of the fluctuating quantity of the dispersed-phase velocity. Numerical experiments with the unsteady drag coefficient in conjunction with 3000, 8000, and 10,000 computational droplets for each representative size were conducted. The predicted evolution of $(\overline{u_p'^2} + \overline{v_p'^2})/2$ for the smallest (10 μm) and largest (80 μm) droplets is presented in Fig. 3 and is compared with the measured data of Liu.[18] Here $\overline{u_{pi}'^2}$ is calculated from

$$\overline{u_{pi}'^2} = \frac{\sum_{m=1}^{M} n_m [(U_{pi})_m - u_{pi}]^2}{\sum_{m=1}^{M} n_m} \tag{19}$$

It is clearly seen that the solution with 3000 computational droplets is not statistically stationary yet, although the solutions with 8000 and 10,000 computational droplets do not differ appreciably from each other. Even for the computation performed with a great number of computational droplets, such as 10,000, which has been shown to achieve nearly a stochastic significant solution, statistical shot noise is still distinctly exhibited in the predicted profiles of $(\overline{u_p'^2} + \overline{v_p'^2})/2$ in Fig. 3. However, 10,000 computational droplets for each representative size will be used for the following computations.

Computation is first performed with the quasisteady drag coefficient. Figures 4 and 5 compare the predicted and measured PDFs of the streamwise and transverse fluctuating velocity components for the droplets with $d_p = 10$ and 80 μm, respectively, at two transverse positions ($y = 1$ and 9 mm) of the streamwise station with $x = 20$ mm. Here the predicted PDF indicates the distribution of the collected number of the computational droplets for various computed u_{pi}' traveling through the cell of a specified grid node. Note that the transverse position of $y = 1$ mm is located inside the shear-layer region of the mixing layer, whereas the transverse position of $y = 9$ mm is located inside the freestream region at this streamwise station. The PDF information of u_{pi}' can provide insight into the two-phase flow dynamics with regard to the turbulent dispersion ability of droplets. Comparisons made in Figs. 4 and 5 reveal that the extent of agreement between the predicted and measured PDF shapes is better for the small droplets ($d_p = 10\,\mu$m) than for the large ones ($d_p = 80\,\mu$m). Let us check a typical condition in

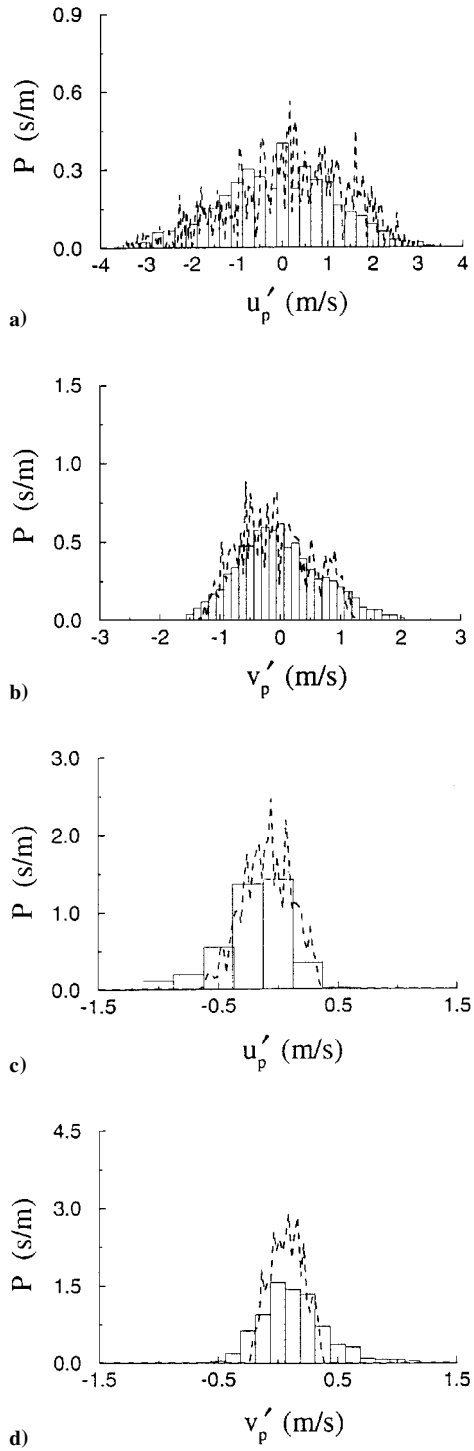

Fig. 4 Comparison of the predicted and measured PDFs for 10-μm droplets using the quasisteady drag coefficient of streamwise and transverse fluctuating velocity components at the 20-mm position: a) u_p', $y = 1$ mm; b) v_p', $y = 1$ mm; c) u_p', $y = 9$ mm; and d) v_p', $y = 9$ mm; $d_p = 10$ μm; vertical bar, measurements,[18] and – – –, steady drag.

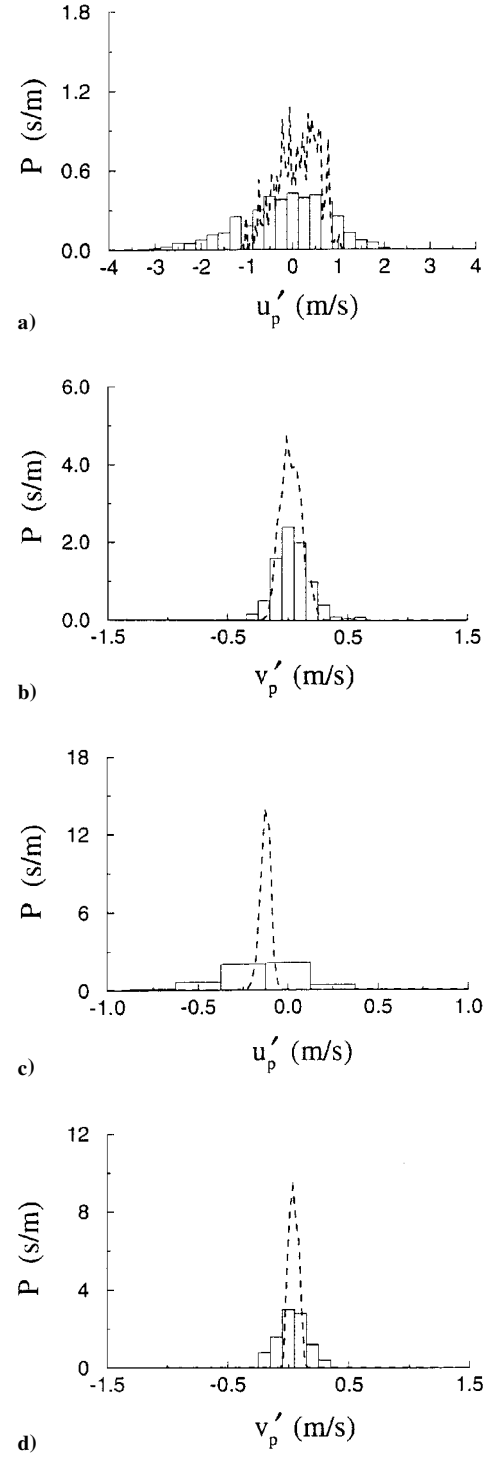

Fig. 5 Comparison of the predicted and measured PDFs for 80-μm droplets using the quasisteady drag coefficient of streamwise and transverse fluctuating velocity components at the 20-mm position: a) u_p', $y = 1$ mm; b) v_p', $y = 1$ mm; c) u_p', $y = 9$ mm; and d) v_p', $y = 9$ mm; $d_p = 80$ μm; vertical bar, measurements,[18] and – – –, steady drag.

the freestream region with these two droplet sizes in the test problem where $|\boldsymbol{U} - \boldsymbol{U}_p| = 1$ m/s, $U_p = 10$ m/s, $\mu = 1.8 \times 10^{-5}$ kg/m · s, $\rho = 1.2$ kg/m^3, and $\rho_p = 1000$ kg/m^3. The values of the factor $\phi(Re)$ for the droplets with sizes of 10 and 80 μm, determined from Eq. (17), are 1.094 and 1.488, respectively. Substitution of Eqs. (4) and (5) into Eq. (2) yields

$$\tau_p = \frac{\rho_p (d_p)^2}{18\mu} \frac{1}{\phi(Re)} \tag{20}$$

showing that τ_p is heavily dependent on the square of d_p. The calculated dynamic relaxation times for the droplets with $d_p = 10$ and 80 μm are, thus, equal to 2.82×10^{-4} and 1.33×10^{-2} s, respectively. For a typical cell with $\Delta x = 2$ mm, the residence time (in seconds) for the specified droplets traveling through the typical cell is approximately estimated by

$$\tau_r = \Delta x / U_p = 2 \times 10^{-4}$$

Obviously, $\mathcal{O}(\tau_p) > \mathcal{O}(\tau_r)$ for the largest droplets, whereas $\mathcal{O}(\tau_p) = \mathcal{O}(\tau_r)$ for the smallest droplets. This means that more large droplets than small droplets cannot reach their steady-state condition when traveling through the grid cell. As a result, the use of the quasisteady drag coefficient in the computations of the PDFs for u_p'

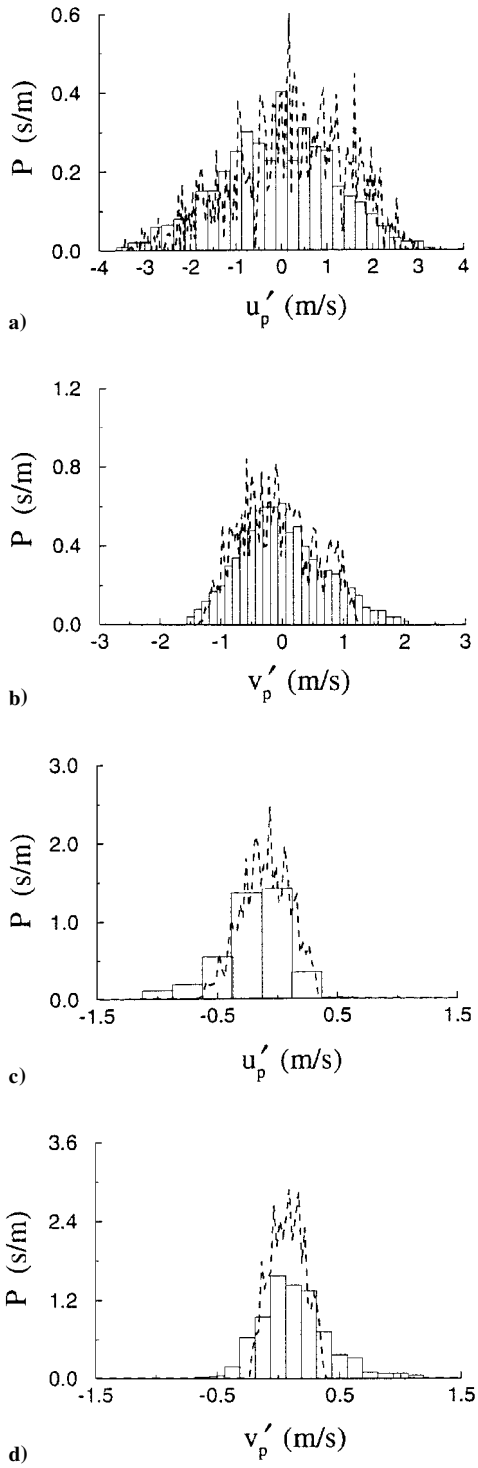

Fig. 6 Comparison of the predicted and measured PDFs for 10-μm droplets using the unsteady drag coefficient of streamwise and transverse fluctuating velocity components at the 20-mm position: a) u_p', $y = 1$ mm; b) v_p', $y = 1$ mm; c) u_p', $y = 9$ mm; and d) v_p', $y = 9$ mm; $d_p = 10$ μm; vertical bar, measurements,[18] and – – –, unsteady drag.

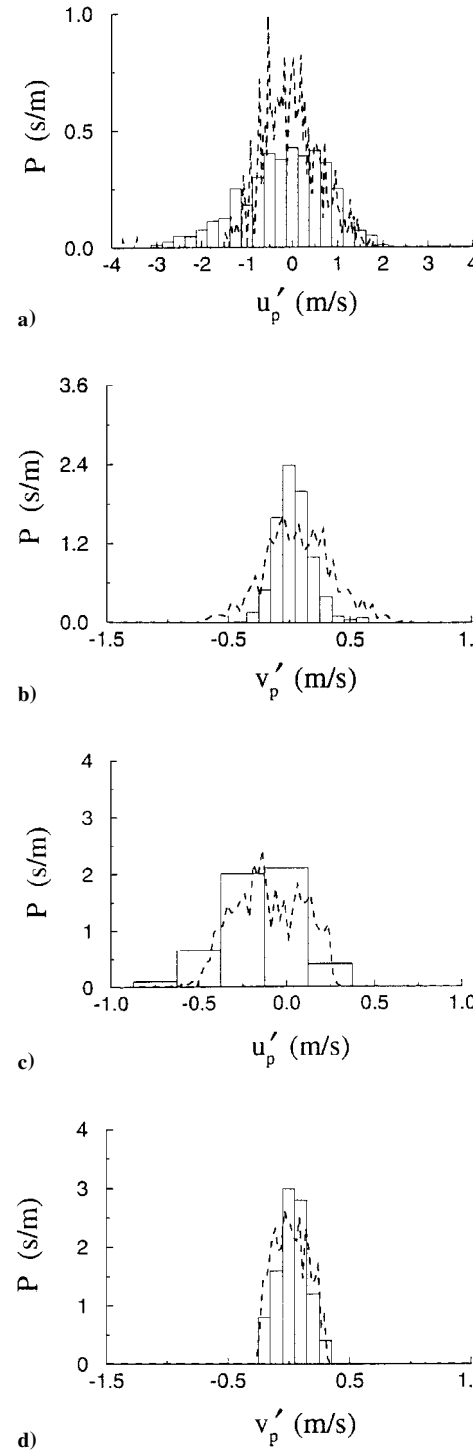

Fig. 7 Comparison of the predicted and measured PDFs for 80-μm droplets using the unsteady drag coefficient of streamwise and transverse fluctuating velocity components at the 20-mm position: a) u_p', $y = 1$ mm; b) v_p', $y = 1$ mm; c) u_p', $y = 9$ mm; and d) v_p', $y = 9$ mm; $d_p = 80$ μm; vertical bar, measurements,[18] and – – –, unsteady drag.

and v_p' yields more significant errors for the large droplets than for the small droplets, as shown in Figs. 4 and 5.

Next the computation is repeated, but with the unsteady drag coefficient described earlier. Figures 6 and 7 show the comparisons between the predicted and measured PDFs of the streamwise and transverse fluctuating velocity components for the droplets with $d_p = 10$ and 80 μm, respectively, at the same two positions of the flowfield. Clearly, the predicted PDF shapes for the large droplets ($d_p = 80\,\mu$m; Fig. 7) are significantly improved by considering the unsteady effect in drag coefficient as compared to the results predicted with the quasisteady drag coefficient shown in Fig. 5. Furthermore, the improvement due to the introduction of the unsteady drag coefficient in the computation for the large droplets seems relatively more effective in the shear-layer region than in the freestream region. This is because the velocity slips between the droplets and the fluid (carrier phase) are usually larger in the shear layer than in the freestream, which leads to larger $\phi(Re)$ values, as computed from Eq. (17), in the shear layer than in the freestream. This, in turn, yields smaller τ_p, as computed from Eq. (20), in the shear layer than in the freestream. According to the foregoing discussion, deviation of the predicted PDF from the measured PDF stemming from the use of the quasisteady drag coefficient in the

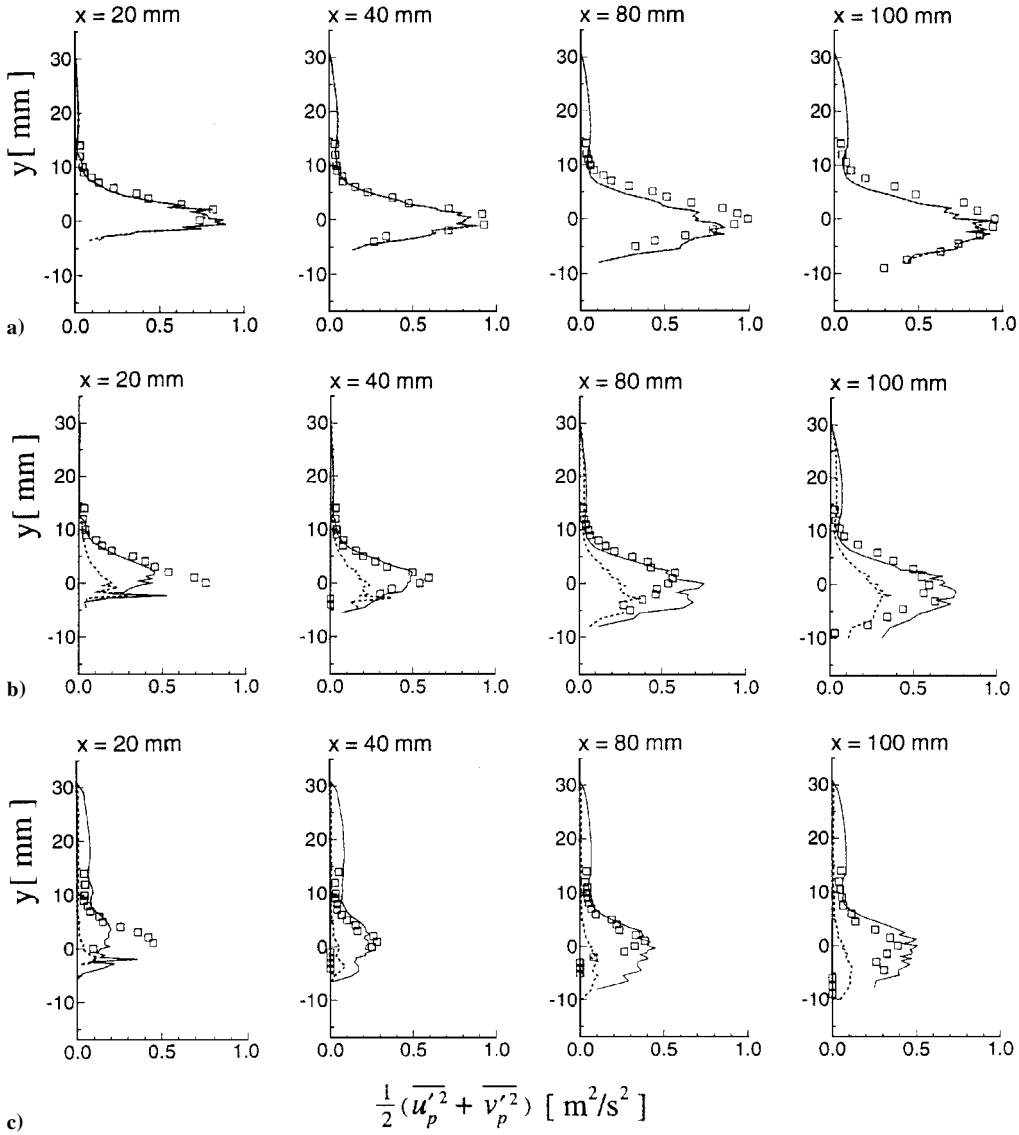

Fig. 8 Evolution of the two predicted (with unsteady and quasisteady drag coefficients) and measured $(\overline{u_p'^2} + \overline{v_p'^2})/2$ of droplets with sizes of a) 10, b) 40, and c) 80 μm: □, measurements[18]; ——, unsteady drag; and – – –, steady drag.

computation should be less as τ_p becomes smaller. In contrast to the result of the large droplets ($d_p = 80\,\mu$m), the PDF shapes predicted with the unsteady and quasisteady drag coefficients for the small droplets ($d_p = 10\,\mu$m) differ only slightly (see Figs. 4 and 6).

The preceding discussion followed from comparisons of the PDF structures at two specified positions of the flowfield (Figs. 4–7). Figure 8 presents the evolution of $(\overline{u_p'^2} + \overline{v_p'^2})/2$ of the droplets with three different sizes predicted with the unsteady and quasisteady drag coefficients in comparison with the measured data of Liu.[18] Note that the selected droplet sizes of 10, 40, and 80 μm here represent the small, medium, and large droplets, respectively, in the investigated two-phase flow problem. However, the same conclusions can be drawn from the results shown in Fig. 8; that is, both the predictions using the unsteady and quasisteady drag coefficients differ slightly from each other and agree well with the measured data for the droplet as small as 10 μm in size, whereas the differences between these two predictions become more remarkable as the droplet size is increased. Another interesting observation made from the comparison in Fig. 8 is that the agreement between the measured data and the prediction using the unsteady drag coefficient is generally good except at the upstream station of $x = 20$ mm for the medium and large droplets only. The following analysis is performed to understand the cause leading to these discrepancies.

The instantaneous droplet velocity component U_{pi} can also be determined by iteratively integrating the nonlinear ordinary differential equation [Eq. (1)] to an acceptable tolerance in a given time step, i.e.,

$$U_{pi} = U_i - [U_i - (U_{pi})_{\text{old}}]\exp(-\Delta t/\tau_p) + g_i\tau_p[1 - \exp(-\Delta t/\tau_p)] \tag{21}$$

where the subscript "old" denotes the value at the beginning of the time increment of Δt. The present computation issues 10,000 computational droplets, which are evenly distributed in the inlet section ($x = 5$ mm). Each computational droplet at the inlet is specified with a number density and a mean droplet velocity component from the measured data.[18,19] Thus, at the first integrating time step as a computational droplet just leaves the inlet position, Eq. (21) becomes

$$U_{pi} = U_i - [U_i - (u_{pi})_{\text{in}}]\exp(-\Delta t/\tau_p) + g_i\tau_p[1 - \exp(-\Delta t/\tau_p)] \tag{22}$$

This is the most conventional treatment of the dispersed-phase inlet condition in the stochastic Lagrangian computations of two-phase flows. An apparent defect, shown in Eq. (22), is that the fluctuating information of the dispersed phase, which is an important turbulent characteristic for the dispersed phase at the inlet, is not considered in the computation. This is the main cause that leads to the significant underestimations of $(\overline{u_p'^2} + \overline{v_p'^2})/2$ obtained with the unsteady drag coefficient in the shear-layer region at the upstream station

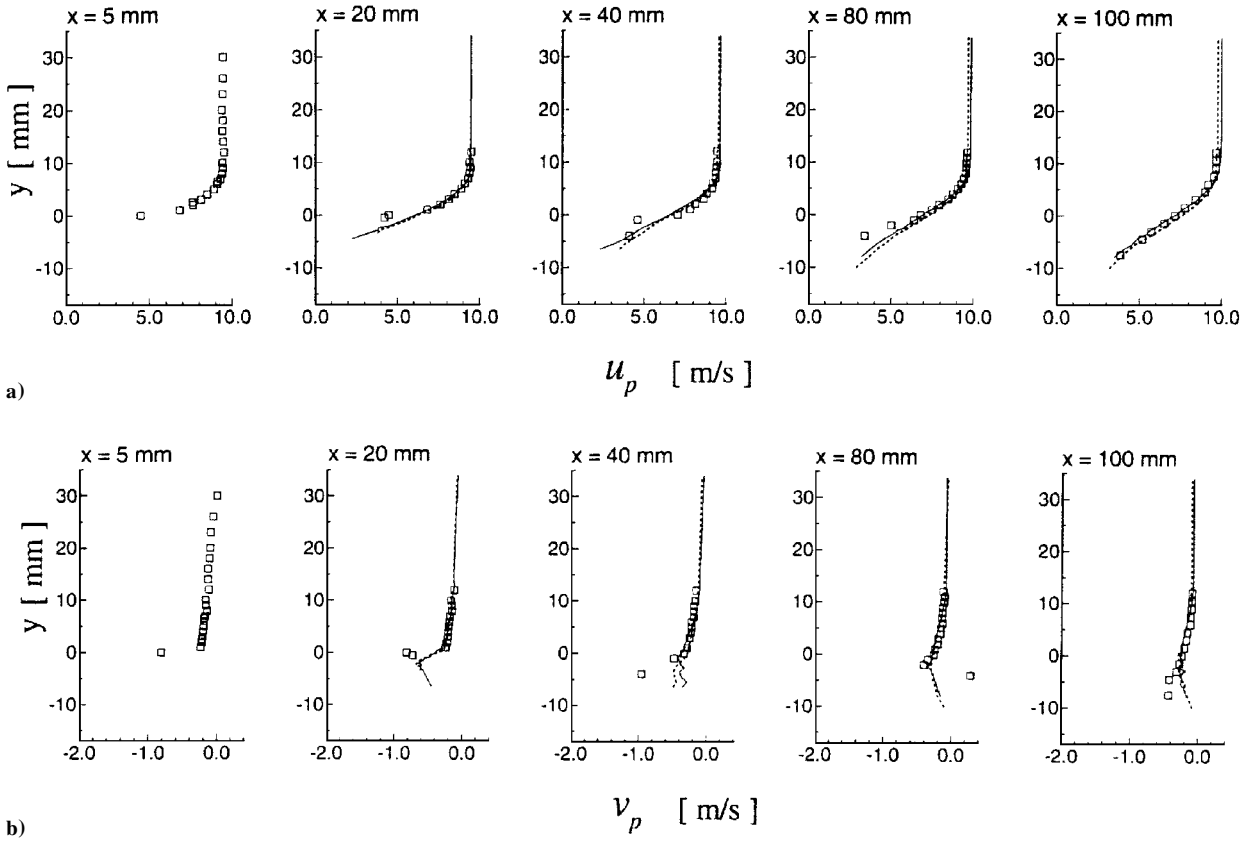

Fig. 9 Evolution of 80-μm droplets of the two predicted (with unsteady and quasisteady drag coefficients) and measured a) mean streamwise and b) mean transverse velocity components: □, measurements[18]; ——, unsteady drag; and – – –, steady drag.

of $x = 20$ mm, as shown in Figs. 8b and 8c, for the medium and large droplets. Note that the values of $(u_{pi}'^2)^{1/2}$ are much higher in the shear-layer region than in the freestream region. Therefore, the neglect of the fluctuating information of the dispersed phase at the inlet should result in more prediction errors of $(u_p'^2 + v_p'^2)/2$ in the shear-layer region than in the freestream region, as shown in Figs. 8b and 8c. It is known that the influence of the inlet condition of turbulence intensity on the single-phase flowfield prediction is appreciable only in the initial region of the flowfield and that it becomes less significant in the downstream region.[22] A similar trend is also observed in Fig. 8. Because the spray was generated at a very upstream location ($x = -950$ mm) in the test problem, this configuration allowed small droplets, such as the one with $d_p = 10\ \mu$m, to be close to the correlative condition with the carrier phase as described by Chang et al.[9] Therefore, no detectable differences between the predicted (with the unsteady C_D) and measured $(u_p'^2 + v_p'^2)/2$ results can be observed even at the upstream station of $x = 20$ mm for this smallest droplet. However, the issue of how to convey the fluctuating information of the dispersed-phase turbulence characteristic at the inlet into the flowfield solution is out of the scope of this study because the present study is focused on the effect of the unsteady drag coefficient in the stochastic Lagrangian computation. This issue remains to be studied in the future.

The results showed that the unsteady effect of the drag coefficient on the prediction of $(u_p'^2 + v_p'^2)/2$ becomes less appreciable as the droplet size is decreased. Only the evolution of the mean streamwise and transverse velocity components of the largest droplet ($d_p = 80\ \mu$m) predicted with the unsteady and quasisteady drag coefficients is presented in Fig. 9 and is compared with the measured result.[18,19] Note that the velocity scales used in Figs. 9a and 9b are different. It is seen that the discrepancies between the two predictions of mean droplet velocity using the unsteady and quasisteady drag coefficients become remarkably less than the discrepancies in their predictions of $(u_p'^2 + v_p'^2)/2$ (see Fig. 8c). Even at the upstream station of $x = 20$ mm, no such appreciable underpredictions of $(u_p'^2 + v_p'^2)/2$ obtained with the unsteady drag coefficient, such as those shown in Fig. 8c, are observed in Fig. 9 for the predictions of mean droplet velocity. The reason is as follows: The mean droplet velocity is computed from the ensemble-averaging formula of Eq. (18), which accounts for the PDF value as the weighting factor. As schematically shown in Fig. 1, the step change of U_i is mainly dominated by the two u_i' values given randomly in two consecutive grid cells. It is clear that the unsteady effect of the drag coefficient on the computation of U_{pi} becomes more appreciable as the step change of U_i is increased. In other words, the greater deviation of U_{pi} from u_{pi} stemmed from the larger u_i', which corresponds to a much smaller PDF value determined by the Gaussian-type PDF used in the work. Thus, although the difference between the two U_{pi} predictions obtained with the unsteady and quasisteady drag coefficients becomes more appreciable as the step change of U_i is increased, this difference is evened out in the determination of u_{pi} by using the ensemble-averaging formula of Eq. (18) due to the weighting effect of the small PDF value.

Because the test problem is a very dilute spray and the differences between the two u_{pi} predicted with the unsteady and quasisteady drag coefficients are slight even for the large droplets, the carrier-phase solution (Eulerian part) is almost invariant in the present computations with and without consideration of the unsteady effect of the drag coefficient. A detailed presentation and discussion on the flow properties of the carrier phase, as well as the small and medium droplets, is given in the work of Chang et al.[19] and is not repeated here.

V. Conclusions

The effect of an unsteady drag coefficient on the conventional stochastic Eulerian–Lagrangian method is examined in a well-defined, droplet loading, planar mixing layer flow. An expression for the unsteady drag coefficient, combining those obtained by Mei and Adrian[16] and Sano,[12] is used in the computation. It is shown that more realistic PDF predictions and improved values of $(u_p'^2 + v_p'^2)/2$ can be achieved through the use of the unsteady drag coefficient rather than the quasisteady drag coefficient. However, the use of

the quasisteady drag coefficient in the stochastic Lagrangian computation does not cause too much deviation in the determination of the mean droplet velocity, as compared with those using the unsteady drag coefficient, through the ensemble-averaging formula of Eq. (18). This work only examined the unsteady effect of drag coefficient in an isothermal two-phase flow problem. The unsteady effects of other interfacial transport properties, such as convection heat and mass transfer coefficients in the evaporating sprays, on the stochastic Lagrangian computation remain to be studied.

Acknowledgment

This work was supported by the National Science Council of the Republic of China under Grant NCHC-86-06-011.

References

[1]Crowe, C. T., Troutt, T. R., and Chung, J. N., "Numerical Models for Two-Phase Turbulent Flows," *Annual Review of Fluid Mechanics*, Vol. 28, 1996, pp. 11–43.

[2]Sirignano, W. A., "Fluid Dynamics of Sprays—1992 Freeman Scholar Lecture," *Journal of Fluids Engineering*, Vol. 118, Sept. 1993, pp. 345–378.

[3]Faeth, G. M., "Mixing, Transport and Combustion in Spray," *Progress in Energy and Combustion Science*, Vol. 13, 1987, pp. 293–345.

[4]Gosman, A. D., and Ioannides, E., "Aspects of Computer Simulation of Liquid-Fueled Combustors," AIAA Paper 81-0323, June 1981.

[5]Chang, K. C., and Wu, W. J., "Sensitivity Study on Monte Carlo Solution Procedure of Two-Phase Turbulent Flow," *Numerical Heat Transfer*, Pt. B, Vol. 25, No. 2, 1994, pp. 223–244.

[6]Dutta, P., Sivathanu, Y. R., and Gore, J. P., "Discrete Probability Function Method for the Calculation of Turbulent Particle Dispersion," *AIAA Journal*, Vol. 35, No. 1, 1997, pp. 200–202.

[7]Chen, X. Q., and Pereira, J. C. F., "Stochastic-Probabilistic Efficiency Enhanced Dispersion Modeling of Turbulent Polydispersed Sprays," *Journal of Propulsion and Power*, Vol. 12, No. 4, 1996, pp. 760–769.

[8]Chen, X. Q., and Pereira, J. C. F., "Efficient Computation of Particle Dispersion in Turbulent Flows with a Stochastic-Probabilistic Model," *International Journal of Heat and Mass Transfer*, Vol. 40, No. 8, 1997, pp. 1727–1741.

[9]Chang, K. C., Wu, W. J., and Wang, M. R., "Limitations of the Stochastic Approach in Two-Phase Turbulent Flow Calculations," *Atomization and Sprays*, Vol. 6, No. 2, 1996, pp. 211–225.

[10]Clift, R., Grace, J. R., and Weber, M. E., *Bubbles, Drops and Particles*, Academic, New York, 1978, Chap. 5.

[11]Michaelides, E. E., "Review—The Transient Equation of Motion for Particles, Bubbles, and Droplets," *Journal of Fluids Engineering*, Vol. 119, No. 2, 1997, pp. 233–247.

[12]Sano, T., "Unsteady Flow Past a Sphere at Low Reynolds Number," *Journal of Fluid Mechanics*, Vol. 112, 1981, pp. 433–441.

[13]Mei, R., "History Force on a Sphere Due to a Step Change in the Free Stream Velocity," *International Journal of Multiphase Flow*, Vol. 19, No. 3, 1993, pp. 509–525.

[14]Lovalenti, P. M., and Brady, J. F., "The Hydrodynamic Force on a Grid Particle Undergoing Arbitrary Time Dependent Motion at Small Reynolds Number," *Journal of Fluid Mechanics*, Vol. 256, 1993, pp. 561–605.

[15]Lovalenti, P. M., and Brady, J. F., "Force on a Body in Response to an Abrupt Change in Velocity at Small but Finite Reynolds Number," *Journal of Fluid Mechanics*, Vol. 293, 1995, pp. 35–46.

[16]Mei, R., and Adrian, R. J., "Flow Past a Sphere with an Oscillation in the Free-Stream and Unsteady Drag at Finite Reynolds Number," *Journal of Fluid Mechanics*, Vol. 237, 1992, pp. 323–341.

[17]Lawrence, C. J., and Mei, R., "Long-Time Behavior of the Drag on a Body in Impulsive Motion," *Journal of Fluid Mechanics*, Vol. 283, 1995, pp. 307–327.

[18]Liu, Y. C., "Transition of the Planar Mixing Layer Under Particle Loading," Ph.D. Dissertation, Inst. of Aeronautics and Astronautics, National Cheng-Kung Univ., Tainan, Taiwan, ROC, Dec. 1991.

[19]Chang, K. C., Wang, M. R., Wu, W. J., and Liu, Y. C., "Theoretical and Experimental Study on Two-Phase Structure of Planar Mixing Layer," *AIAA Journal*, Vol. 31, No. 1, 1993, pp. 68–74.

[20]Patankar, S. V., *Numerical Heat Transfer and Fluid Flow*, McGraw–Hill, New York, 1980, Chap. 6.

[21]Fehlberg, E., "New High-Order Runge–Kutta Formula with an Arbitrarily Small Truncation Error," *Zeitschrift fur Angewandte Mathemetik and Mechanik*, Vol. 46, 1966, pp. 1–16.

[22]Chang, K. C., and Chen, C. S., "Influence of Inlet Boundary Conditions on Turbulent Flowfield Computation," *International Journal of Turbo and Jet Engines*, Vol. 9, No. 1, 1992, pp. 11–28.

J. P. Gore
Associate Editor